The Pennsylvania State University

The Graduate School

Intercollege Graduate Degree Program in Molecular Medicine

BIOCONJUGATION OF CALCIUM PHOSPHATE NANOPARTICLES FOR SELECTIVE TARGETING OF HUMAN BREAST AND PANCREATIC CANCERS *IN VIVO*

A Thesis in

Molecular Medicine

by

Rahul Sharma

Submitted in Partial Fulfillment
of the Requirements
for the Degree of

Master of Science

August 2009

The thesis of Rahul Sharma was reviewed and approved* by the following:

James H. Adair
Professor of Materials Science and Engineering
Thesis Adviser

Kouacou Konan
Assistant Professor of Biochemistry and Molecular Biology

Avery August
Professor of Immunology
Co-Chair, Intercollege Graduate Degree Program in Molecular Medicine

*Signatures are on file in the Graduate School

ABSTRACT

This study describes the design and synthesis of targeted calcium phosphate nanoparticles (CPNPs) through bioconjugation of human holotransferrin, anti-CD71 antibody, and short gastrin peptides via avidin-biotin- or PEG-maleimide-coupling strategies. Furthermore, this study evaluates the specificity of these targeted CPNPs *in vivo* in models of breast and pancreatic cancer. These bioconjugated CPNPs potentially permit enhanced drug delivery, targeting and imaging of breast and pancreatic cancer tumors. This is the first report on avidin-conjugated CPNPs for use in improving cellular uptake. The conjugation of biotinylated human holotransferrin (diferric transferrin) and biotinylated anti-CD71 antibody (anti-transferrin receptor antibody) to avidin conjugated CPNPs (avidin-CPNPs) permits targeting of the transferrin receptor on cells. Early studies have shown that the transferrin receptor is specifically over-expressed on breast cancer cells in comparison to healthy cells. Thus, conjugation of biotinylated human holotransferrin or biotinylated anti-CD71 antibody to avidin-CPNPs can potentially be utilized to enhance the targeting of breast cancer. In a manner similar to targeting breast cancer via the transferrin receptor (CD71), the conjugation of biotinylated pentagastrin to avidin-CPNPs and gastrin-10 to PEG-CPNPs via PEG-maleimide coupling permits for targeting of the gastrin receptor; gastrin receptor expression is often increased in pancreatic cancer. This study demonstrates that these targeting

strategies can potentially increase the uptake efficiency of CPNPs by breast and pancreatic cancer cells and increase the specificity of CPNPs for these cancer cells, which would decrease the systemic toxicity to normal cells, as a result of reduced amount of toxic anti-cancer drugs in the extracellular fluid.

TABLE OF CONTENTS

LIST OF FIGURES vi

ACKNOWLEDGMENTS ix

Introduction 1

Experimental Procedures 7

Results and Discussion 18

Conclusions 31

References 33

LIST OF FIGURES

Figure 1. Illustration of the dissolution mechanism of CPNPs during receptor-mediated endocytosis……..……..3

Figure 2. Solubility of calcium phosphates as a function of pH….....……..…6

Figure 3. The reaction scheme for the 2,6-ANS assay to evaluate avidin bioconjugation on the CPNPs ……..……...15

Figure 4. A: Zeta potential distributions for citrate-CPNPs, PEG-CPNPs, and avidin-CPNPs. The citrate-CPNPs (blue line) displayed a mean zeta potential of -16 ± 1.3 mV, whereas, the avidin-CPNPs (green line) had a mean zeta potential value of +29 ± 8.7 mV. In some cases, the zeta potential was as high as +39.8 ± 5.5 mV. The PEG-CPNPs (red line) displayed a mean zeta potential of +3.0 ± 2.0 mV. All zeta potential distributions are representative of three independent experiments. B: Dynamic light scattering determinations for citrate-CPNP, Anti-CD71-Av-CPNP: Anti-CD71-Avidin-CPNPs, PG-Av-CPNP: Pentagastrin-Avidin-CPNPs, and Tf-Av-CPNP: Human Holotransferrin-Avidin-CPNPs. All dynamic light scattering determinations are the mean of three independent experiments……....….19

Figure 5. TEM images of A: Citrate-CPNPs; B: Anti-CD71-Avidin-CPNPs; C: Human Holotransferrin-Avidin-CPNPs; D: Pentagastrin-Avidin-CPNPs.……21

Figure 6. The displacement of 2,6-ANS was utilized to evaluate the coupling of biotin to avidin-CPNPs. A: Fluorescence intensities for the first step of the 2,6-ANS

assay. The addition of 2,6-ANS to the avidin-CPNP complex results in a six fold increase in fluorescence as the fluorescent probe binds to the biotin binding site on avidin. The 2,6-ANS was added at increasing concentrations to avidin-CPNPs and increased fluorescence, indicative of 2,6-ANS bound to avidin, was quantitatively determined. B: Peak height of fluorescence shown on Figure 6A as a function of 2,6-ANS molarity. C: Fluorescence intensities for the second step of the 2,6-ANS assay. The addition of biotin to the 2,6-ANS-Avidin-CPNP complex results in a decrease in fluorescence as biotin displaces the fluorescent probe from the biotin binding site on avidin. Biotin was added at increasing concentrations to the 2,6-ANS-Avidin-CPNP complex and a decrease in fluorescence, indicative of biotin displacing 2,6-ANS, was quantitatively determined. D: Peak height of fluorescence shown on Figure 6C as a function of biotin molarity. All determinations are representative of three independent experiments……..……23

Figure 7. Targeting transferrin receptors in an *in vivo* subcutaneous-tumor model of breast cancer. Human MDA-MB-231 metastatic breast cancer cells were xenografted subcutaneously into athymic nude mice. One week following engraftment, ICG-loaded CPNPs were administered systemically via tail vein injection and near-infrared images were taken 96 hours post-injection. From left to right, mice receiving: (i) free ICG, (ii) ICG-loaded, PEG-CPNPs, (iii) ICG-loaded, Anti-CD71-Avidin-CPNPs, or (iv) ICG-loaded, Human Holotransferrin-Avidin-CPNPs. Inserts: excised tumors (mice ii, iii, and iv), excised spleen (mouse iii). All images are representative of four independent experiments……..……..…27

Figure 8. Targeting gastrin receptors in an *in vivo* orthotopic-tumor model of pancreatic cancer. Human BxPC-3 pancreatic cancer cells were xenografted orthotopically into athymic nude mice. One week following engraftment, ICG-loaded CPNPs were administered systemically via tail vein injection and near-infrared images were taken 96 hours post-injection. From left to right, mice receiving: (i) ICG-loaded, PEG-CPNPs, (ii) ICG-loaded, Gastrin-10-PEG-CPNPs (covalently coupled), or (iii) ICG-loaded, Pentagastrin-Avidin-CPNPs. Respective inserts to all mice: (panc) excised, tumor-bearing, pancreas, and (stom) excised stomach. All images are representative of at least four independent experiments ..……..……29

ACKNOWLEDGEMENTS

I wish to thank Keystone Nano, Inc. for partial support of my M.S. thesis research. I also wish to acknowledge Dr. James H. Adair and Dr. Avery August for their contributions as co-advisors on my thesis research. The support and guidance of my fellow students in the Adair group, Thomas T. Morgan and Erhan I. Altinoğlu, is also deeply appreciated. The support from our research collaborators at Hershey Medical Center in the Departments of Pharmacology and Medicine, Dr. Brian M. Barth, Dr. Mark Kester, Dr. Jill P. Smith, and Chris McGovern, where the maleimide mediated bioconjugation and the *in vivo* studies took place, is also acknowledged with gratitude.

Introduction

Calcium phosphate nanoparticles (CPNPs) have been engineered to be a non-toxic vehicle for the delivery of a diversity of therapeutic and imaging agents in biological systems (Morgan et al., 2008; Altinoğlu et al., 2008; Kester et al., 2008; Muddana et al., 2009). Previous studies have shown that encapsulation within CPNPs improved the lifetime and quantum properties of fluorescent dyes (Morgan et al., 2008). Initial *in vivo* imaging trials demonstrated that CPNPs, functionalized with polyethylene glycol (PEG) moieties, accumulated within solid tumors via an enhanced permeation retention (EPR) effect (Altinoğlu et al., 2008). While EPR serves as an effective passive targeting strategy, particular interest lies in the ability to target cancerous cells to deliver anti-neoplastic agents, thereby decreasing effective dosage and limiting off-target toxicity. Recent research has showed increased expression of certain surface features on cancerous cells, a circumstance that can be exploited to target CPNPs.

Of particular interest is the prevalence of transferrin receptors (CD71) on cancerous cells, including breast cancer. The transferrin receptor is responsible for transporting iron, via interaction with transferrin, into cells as demanded by metabolic need. Accordingly, transferrin receptors are found predominately on proliferating cells, including many cancerous cells as well as hematopoietic cells.

The transferrin receptor is specifically over-expressed on breast cancer cells for several reasons. Breast cancer cells are metabolically hyperactive, have deregulated cell growth, and have increased demand for iron (Omary et al., 1980; Sutherland et al., 1981; Shindelman et al., 1981; Daniels et al., 2006a; Daniels et al., 2006b). All of these characteristics and processes involved in breast cancer metabolism necessitate the presence of additional transferrin receptors on the cell membrane to adequately meet the elevated demands of the transformed cancer cell. As a result, the transferrin receptor is over-expressed.

At pH 7.4, the CPNPs are sparingly soluble, but, at pH 5 the CPNPs dissolve (Morgan et al., 2008, Muddana et al., 2009). This property of CPNPs is important for receptor mediated drug delivery and the development of bioconjugated CPNPs. During transferrin receptor-mediated endocytosis there is a drop in the internal pH of the endosome when the resulting endosome containing the Anti- CD71- or Human Holotransferrin-Avidin-CPNP complex is formed (Figure 1).

The internal pH of the endosome drops from approximately pH 7.4 to pH 4 - 5 because the newly formed endosome contains a functional proton pump which pumps H^+ into the endosome (Panyam et al., 2003). Thus, the internal pH of the endosome decreases (Panyam et al., 2003). This is a physiological process that occurs during Fe^{3+} transport into cells. The change in pH of the endosome from neutral to acidic permits the release of Fe^{3+} from the holotransferrin. The released Fe^{3+} is then reduced to Fe^{2+} and transported out of the endosome by an iron transporter called divalent metal transporter 1 (DMT1) (Daniels et al., 2006a;

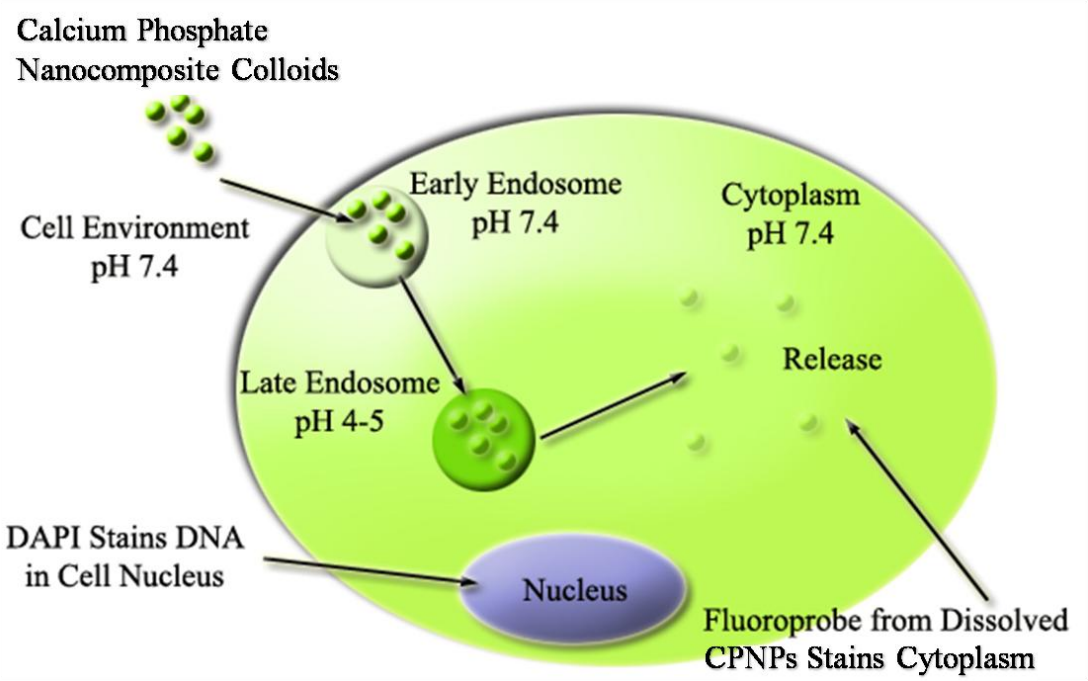

Figure 1. Illustration of the dissolution mechanism of CPNPs during receptor-mediated endocytosis (Modified from: Panyam J, Labhasetwar V. Adv Drug Deliv Rev. 2003;55(3):329-47).

Daniels et al., 2006b). Since the CPNPs dissolve in the acidic environment of the endosome, the CPNPs release the encapsulated agent (anti-cancer drug or imaging probe) inside the endosome. The pH response of CPNPs produces two effects. First, it permits a decrease in the effective dose of chemotherapeutic drugs, which are often toxic, required for optimal therapeutic benefit by increasing the efficiency of drug delivery into cancer cells (Kester et al., 2008). Second, it decreases the amount of drug present in the extracellular fluid where the pH is maintained at approximately 7.4 by physiological buffers. At physiological pH, the bioconjugated CPNPs are

colloidally stable and do not dissolve. Thus, the drug encapsulated in the CPNPs is not released into the extracellular fluid. This is an important advantage since it decreases the systemic toxicity to healthy cells because the extracellular fluid no longer serves as a transport medium for the drug into healthy cells.

In a manner similar to CD71, gastrin receptors have a predominate prevalence within certain tissues, specifically the gastrointestinal and central nervous systems (Smith et al., 1995; Smith et al., 1996; Wank et al., 1992). The hormone gastrin binds to a family of G-protein-coupled receptors, also known as the cholecystokinin-2 (CCK_2 or CCK-B) receptor family, and is typically known as a key mediator of stomach acidity and gastric motility. Intriguingly, CCK_2 receptor expression is often increased in many cases of gastrointestinal cancer, including pancreatic cancer, and in particular, an increase in the expression of a specific splice variant (CCK_{2i4sv} or CCK-C) of the receptor.

In the present work, an active agent, the near infra-red emitting fluorophore, indocyanine green (ICG), is encapsulated within the CPNPs. Previous studies have shown that various properties of calcium phosphate, including the surface chemistry, chemical composition, particle size, porosity, structure and morphology play an important function in determining the initial encapsulation efficiency of anti-cancer drugs, the subsequent delivery efficiency of the anti-cancer drug to its target site – cancer cells and the entire time period over which this process occurs (Barroug et al., 2002; Bajpai et al., 1988; Barroug et al., 1997; Barroug et al., 1989; Barroug et al., 1992). It has been shown that variations in the calcium to phosphate ratio may be

utilized to predetermine the kinetics of dissolution of nanoparticles by controlling the phase of the calcium phosphate at a given time (Magne et al., 2002, Panyam et al., 2003). This is feasible since the solubility of calcium phosphate varies for the different phases of calcium phosphate, which vary as a function of pH (De Groot et al., 1990; Rouse, 2006; Tung, 1998) (Figure 2). Amorphous calcium phosphate has a higher solubility than any of the crystalline phases of calcium phosphate shown on Figure 2, but it is a poorly defined system. Nevertheless, amorphous calcium phosphate follows the same trend in solubility with respect to pH as the other phases of calcium phosphate. In aqueous solution at a pH less than 4.2, the dicalcium phosphate phase is the most stable phase. In contrast, at a pH greater than 4.2, the hydroxyapatite phase is the most stable phase. At pH 7.4 (physiological pH), the solubility of the calcium phosphate phases decreases in the order of amorphous calcium phosphate > dicalcium phosphate dihydrate (brushite) [$CaHPO_4 \bullet 2H_2O$] > dicalcium phosphate anhydrous [$CaHPO_4$] > tricalcium phosphate [$Ca_{3(}PO_4)_2$] > hydroxyapatite [$Ca_5(PO_4)_3OH$]. In fact, the amorphous calcium phosphate nanoparticles (CPNPs) used in this study dissolve below pH 7.4 (Morgan et al., 2008; Altinoğlu et al., 2008; Kester et al., 2008; Muddana et al., 2009). The primary reason for this dependence of the solubility of calcium phosphates on the pH of the solution is that phosphoric acid is a weak acid, as well as a polybasic acid. As a result of these characteristics of phosphoric acid, any variations in the pH of the solution cause a significant variation in the concentrations of HPO_4^-, $H_2PO_4^{2-}$, and PO_4^{3-} (Tung, 1998). These characteristics of calcium phosphate are valuable for

tuning the synthesis to prepare nanoparticles whose solubility is predetermined to meet the needs of a particular nanomedical application.

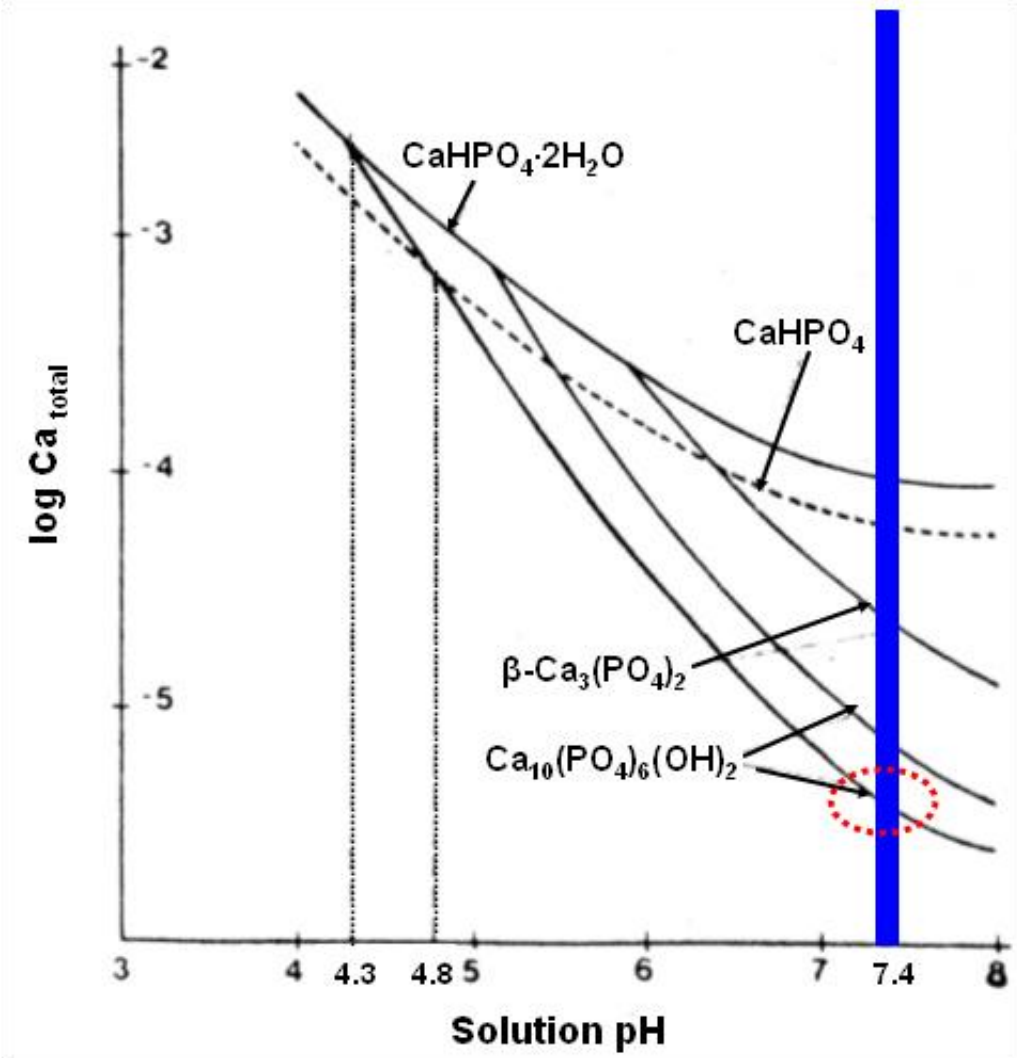

Figure 2. Solubility of calcium phosphates as a function of pH (Modified from: De Groot K, Klein CPAT, Wolke JGC, de Blieck-Hogervors JMA. CRC Press: Boca Raton, 1990;3–17 and Rouse SM. Ph.D. dissertation, 2006).

Experimental Procedures

Preparation of Nanoparticles

CPNPs were prepared by the microemulsion technique and van der Waals-HPLC that have been previously described (Morgan et al., 2008; Altinoğlu et al., 2008; Kester et al., 2008; Muddana et al., 2009). Cyclohexane (C_6H_{12}, 99%, BHD Chemical Co.), Igepal CO-520 ($C_{13}H_{20}O(C_2H_4O)_{n=5}$, Rhodia Chemical Co.), and deionized H_2O were used to prepare the microemulsions. Calcium chloride ($CaCl_2.2H_2O$, Sigma-Aldrich Co.), disodium hydrogen phosphate (Na_2HPO_4, Sigma Aldrich Co.), and sodium metasilicate (Na_2SiO_3, Sigma-Aldrich Co.) were used as particle precursors. Disodium hydrogen citrate dihydrate ($HOC(COOH)(CH_2COONa)_2 \cdot 2H_2O$, Sigma-Aldrich Co.) was used as the dispersant. Indocyanine green (ICG) (TCI America Co.) was used as the dopant fluorophore in the CPNPs. Neat ethanol was purchased from VWR International. All other chemicals were obtained from Sigma-Aldrich Co., unless otherwise noted.

Two separate Microemulsions (1 and 2) were formed with a cyclohexane/Igepal CO-520/water system. The molar ratio of water to surfactant was 4. A 650 μL of 1 x 10^{-2} M $CaCl_2$ in CO_2-free deionized H_2O was added to 14 mL of a 29 volume percent solution of Igepal CO-520 in cyclohexane to form Microemulsion 1. Similarly, 65 μL of 6 x 10^{-2} M disodium hydrogen phosphate

(Na_2HPO_4) with 65 μL of 8.2 x 10^{-3} M sodium metasilicate (Na_2SiO_3) in CO_2-free deionized H_2O (pH 7.4) was added to 14 mL of a 29 volume percent solution of Igepal CO-520 in cyclohexane to form Microemulsion 2. A 520 μL aliquot of 0.01 M ICG in CO_2-free deionized H_2O was added into Microemulsion 2 so that the final H_2O volume matched that in Microemulsion 1 (650 μL), hence retaining the water to surfactant ratio in each. The individual microemulsions were allowed to equilibrate for 1 hour before 1 and 2 were mixed to form Microemulsion 3. Microemulsion 3 was allowed to undergo micellar exchange for 2 minutes, during which time doped CPNPs precipitated in the micelles. A 225 μL aliquot of 1 x 10^{-2} M sodium citrate was added to Microemulsion 3 and allowed to react for 15 minutes. After adding the dispersant, the reverse micelles were dissolved with 50 mL of ethanol adjusted with 1 M KOH before laundering via the van der Waals-HPLC (Morgan et al., 2008; Altinoğlu et al., 2008; Kester et al., 2008; Muddana et al., 2009).

The unwashed CPNP suspension was loaded onto a silica HPLC (high performance liquid chromatography) column after the micelles had been dissolved with ethanol; the free organic was laundered with ethanol adjusted with 1 M KOH as the eluent; finally, the particles were eluted using 70:30 ethanol:water by volume. During the washing step, the dye content was monitored at an absorption of 785 nm. The ethanol washing was continued until the detector reached baseline indicating removal of the Igepal CO-520 amphiphile. The particles were then eluted with a 70:30 ethanol:water solution. The first major peak was collected. The precursor and HPLC solutions were prepared with CO_2-free deionized H_2O to avoid carbonate

contamination in the CPNPs. All solution pH measurements were performed using a Sentron ISFET pH probe calibrated against aqueous standards.

To bioconjugate the CPNPs with avidin (Scheme 1A), a 1 mL aliquot of CPNPs in their 70% ethanol solution were first dried under argon and covered from light until all solution evaporated and only solid CPNPs remained. This dried sample was then reconstituted back to 1 mL with the addition of 1 mL 1X PBS (0.01 M Phosphate buffer, 0.14 M NaCl, 0.01 M KCl at pH 7.4). This was then followed by the addition of 1 mL of 20 mg/mL 1-ethyl-3-[3-dimethylaminopropyl]-carbodiimide hydrochloride (EDCI) (Sigma-Aldrich Co.) and 1 mL of 6 mg/mL avidin (Rockland Immunochemicals Inc.). Excess avidin was added in order to ensure the surface saturation of CPNPs. This reaction mixture was finally incubated at 35°C for 24 hours in the dark with continuous stirring at 600 RPM.

After 24 hours, the reaction mixture was centrifuge filtered with a 100 kDa centrifuge filter device (Amicon Ultra-4, PLHK Ultracel-PL Membrane; Millipore Co.) to remove excess unconjugated avidin. Prior to use, the filtration membrane of the centrifuge filter device was washed with deionized H_2O in order to minimize non-specific binding. A total of three centrifuge filtrations, each at 1000 x g for 30 minutes, were performed in order to maximize the removal of excess unconjugated avidin. After each centrifuge filtration step, the final volume of the retentate solution was brought back to the starting volume by the addition of 1X PBS.

Multiple types of commercially available centrifuge filter devices, with different filtration membrane materials and chemistry, were evaluated to obtain

minimal non-specific adsorption and optimal washing of the CPNPs. The Millipore Amicon centrifuge filter device with 100 kDa nominal molecular weight limit Ultracel YM-100 regenerated cellulose membrane was identified as the product of choice. Centrifuge filter devices with a polyethersulfone filtration membrane were not feasible for this investigation due to significant non-specific binding of the CPNPs to the filtration membrane.

The conjugation of biotinylated human holotransferrin or biotinylated anti-CD71 antibody to avidin-CPNPs permits targeting of the transferrin receptor; the conjugation of biotinylated pentagastrin to avidin-CPNPs permits targeting of the gastrin receptor (Scheme 1B). A 1 mL aliquot of 3.2 mg/mL biotin conjugated human holotransferrin (Invitrogen Co.), 0.20 mL of 1 mg/mL biotin conjugated anti-CD71 antibody (GeneTex Inc.), or 0.50 mL of 1 mg/mL biotin conjugated pentagastrin (Bachem Co.) (in 0.1 N NH_4OH) was added to 1 mL of avidin-CPNP complex. This reaction mixture was stirred at 600 RPM for 60 minutes at room temperature. The resulting biomolecule-Avidin-CPNP complex was then filtered to remove excess unconjugated biomolecule (human holotransferrin, anti-CD71 antibody, or pentagastrin). Human holotransferrin-Avidin-CPNPs and anti-CD71-Avidin-CPNPs were filtered by tangential flow diafiltration using a 500 kDa molecular weight cut-off (MWCO) MicroKros hollow fiber tangential flow diafiltration device (Spectrum Laboratories Inc.). Pentagastrin-Avidin-CPNPs were centrifuge filtered with a 100 kDa centrifuge filter device (Amicon Ultra-4, PLHK Ultracel-PL Membrane; Millipore Co.). All the biomolecule-Avidin-CPNP samples

were filtered three times in order to maximize the removal of excess unconjugated biomolecule. After each filtration step, the final volume of the retentate solution was brought back to the starting volume by the addition of 1X PBS.

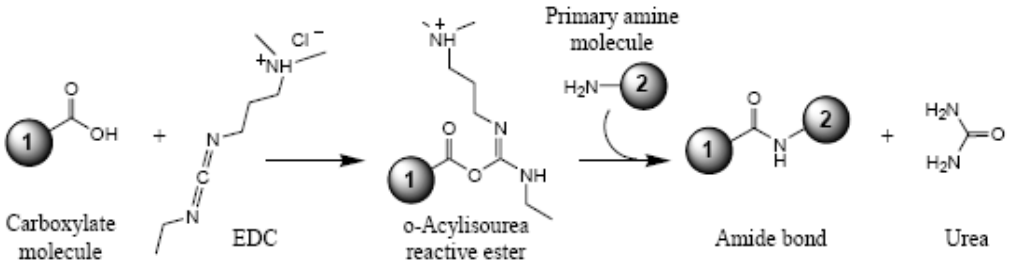

Citrate-CPNP Avidin Avidin-CPNP

Scheme 1A. Step 1 of Avidin-Biotin coupling strategy using an EDCI linker which facilitates the conjugation of avidin to citrate-CPNP by activating the carboxylate moiety on citrate-CPNP (Modified from: EDCI technical notes, Pierce Biotechnology).

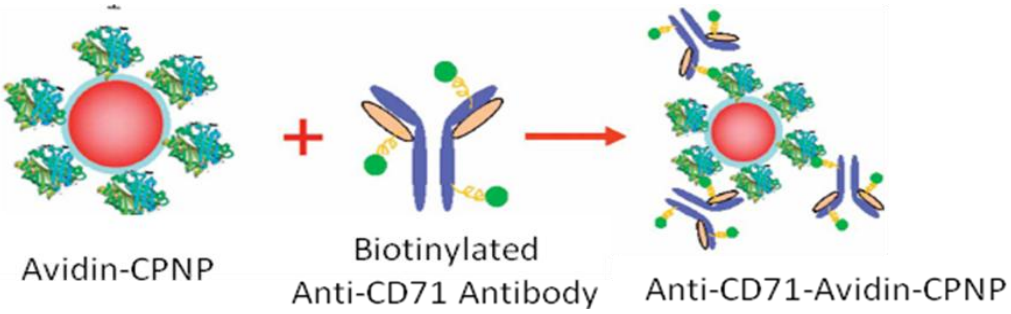

Scheme 1B. Step 2 of Avidin-Biotin coupling strategy with biotin groups on the antibody binding to avidin-CPNP (Modified from: Xing Y. et al., Nat Protoc. 2007;2(5):1152-65).

The conjugation of gastrin-10 to CPNPs via the PEG-maleimide coupling strategy (Scheme 2) permits targeting of the gastrin receptor. A 9 mL aliquot of citrate-CPNPs was chemically conjugated with maleimide polyethylene glycol amine (JenKem Technology Inc.) (PEG-maleimide), through the ethyl-N-(3-dimethylaminopropyl)-N' hydrochloride carbodiimide reaction (EDCI, Fluka BioChemika ≥99.0% (AT); Sigma-Aldrich Co.). The sample was first stirred at 550 RPM on a combined magnetic stir/hot plate set to 50^{o}C. In a drop wise manner, 1 mL of EDCI (1 mg/mL) followed by 1 mL of PEG-maleimide (10 mg/mL), both in aqueous solutions of CO_2-free deionized H_2O (pH 7), were added to the sample under continuous stirring, to produce a calculated 6-fold excess for monolayer surface coverage. The particles were left to react for 15 hours at 50^{o}C to form amide linkages between the carboxylate surfaces and the PEG-maleimide. The mixture was then centrifuge filtered through a 100 kDa filter (Amicon Ultra-4, PLHK Ultracel-PL Membrane; Millipore Co.) at 5000 x g for 2 minutes to remove any excess EDCI and unreacted PEG-maleimide. The characterization of the resulting maleimide-PEG-CPNPs in the retentate showed that the CPNPs remained well dispersed after the centrifugation wash. The gastrin-10 peptide has a cysteine residue for covalent attachment. Thus, the gastrin-10 was added at a 5:1 molar excess to the maleimide-PEG-CPNPs. This solution was incubated overnight at 4 °C, protected from light, to produce Gastrin-10- PEG-CPNPs.

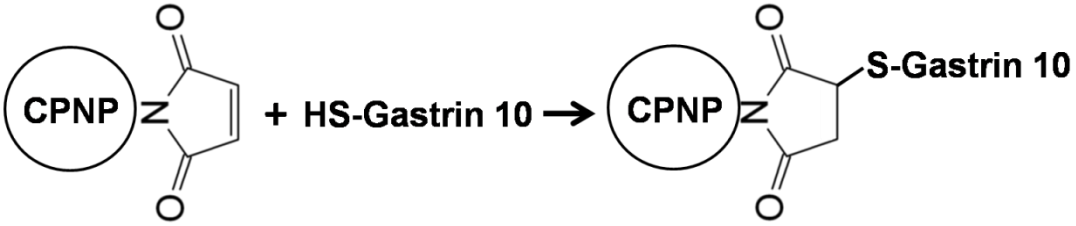

Maleimide-PEG-CPNP Gastrin-10-PEG-CPNP

Scheme 2. PEG-maleimide coupling strategy for CPNPs with a maleimide terminal group on a PEG linker interacting with a terminal sulfhydryl group on a gastrin-10 molecule.

Physical Characterization of Nanoparticles

Particle size distributions for the CPNPs were obtained through dynamic light scattering (DLS) using a Malvern Nano-S Zetasizer. Transmission electron microscopy (TEM) was performed using a JEOL JEM 1200 EXII instrument on dried nanoparticles prepared on a carbon film grid with a copper backing. To verify that avidin was grafted on the CPNPs, zeta potential distributions were obtained using a Brookhaven ZetaPALS zeta potential analyzer. To quantify and test the bioactivity of avidin grafted on CPNPs, a fluorometric assay for avidin-biotin interaction based on the displacement of the fluorescent probe 2-Anilinonaphthalene-6-sulfonic acid (2,6-ANS) was utilized (Mock et al., 1985). The reaction scheme for the 2,6-ANS assay is illustrated in Figure 3.

A 4.85 mg/mL solution of 2,6-ANS (Molecular Probes, Invitrogen Co.) was prepared in 1 mL of deionized H_2O. A 24 µg/mL solution of biotin was prepared in 10 mL of deionized H_2O to produce the biotin solution for the assay. The 2,6-ANS solution, followed by the biotin solution, was titrated in 0.50 µl aliquots into the avidin-CPNP solution to obtain a sufficient number of data points. The reaction mixture was stirred for one minute after the addition of each aliquot to the avidin-CPNP solution to allow enough time for a homogeneous reaction mixture and to maintain consistency with respect to reaction time throughout the experiment.

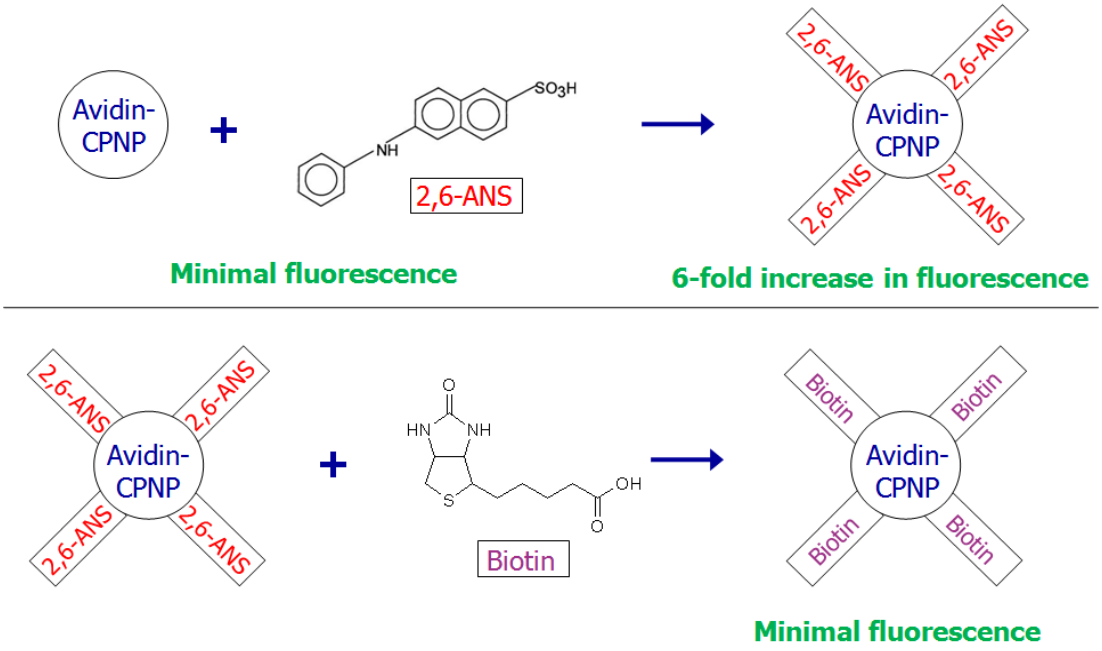

Figure 3. The reaction scheme for the 2,6-ANS assay to evaluate avidin bioconjugation on the CPNPs.

The fluorescence spectra were recorded with a PTI fluorometer in which emitted radiation is collected at 90 degrees with a photomultiplier tube (PMT) detector. The sample is excited by a xenon arc lamp whose illumination passes through a 5 nm bandwidth slit and a monochrometer to select the excitation wavelength. For the emission scan, the excitation wavelength was set to 328 nm and the emission wavelength range was set to 350 – 625 nm.

In Vivo Evaluation of Nanoparticles

The general method used for the *in vivo* animal studies has been described in detail previously (Altinoğlu et al., 2008). In brief, nude mice were obtained from Harlan Co. and all animal protocols were approved by the Pennsylvania State University Institutional Animal Care and Use Committee. Sterile technique was used for all animal protocols. The cells were cultured in DMEM supplemented with 10% fetal bovine serum (FBS). Trypsin/EDTA was used to detach the exponentially growing cells from the tissue culture plate. The cells were resuspended in 1X PBS before being injected at approximately 10^6 cells/mouse. An *In Vivo* FX whole animal imaging station (Kodak Co.) was used to obtain the near-infrared transillumination images. The mice were put into the imaging chamber, and inhalation of 5% IsoSol vapor (isoflurane, Vedco Co.) in 100% oxygen was used to induce and maintain anesthesia. A 755 nm bandpass excitation and 830 nm bandpass emission filter set was used to obtain a 3 minute exposure under near-infrared excitation. An underlying reference was obtained as a 1 second exposure X-ray image of the mice in the same position. The signal distribution relative to anatomy was illustrated by merging the separate near-infrared fluorescence and X-ray images. For each time point over a 96 hour period, the anesthesia and imaging procedure was repeated. The Kodak MI imaging software (Kodak Co.) was used to

pseudocolor the near-infrared images and merge them with the underlying reference X-ray images.

To evaluate the breast cancer-targeted CPNPs *in vivo*, xenografted MDA-MB-231 human breast cancer cells (American type Culture Collection) injected subcutaneously into athymic nude mice were used. Once the tumors established (one week), CPNPs suspended in sterile isotonic saline were injected into the tail veins of the mice, and routine images were taken over a 96 hour period. As controls, free ICG or ICG-loaded, PEG-CPNPs (non-targeted) were alternatively injected, these were diluted to ensure that equivalent ICG concentrations (as determined by absorption spectroscopy) were administered to each mouse. This experiment was repeated four times.

To evaluate the pancreatic cancer-targeted CPNPs *in vivo*, an *in vivo* model of pancreatic cancer, BxPC-3 human pancreatic cancer cells (American type Culture Collection), were orthotopically xenografted into the pancreas of athymic nude mice. This model also allowed the further evaluation of the efficacy of the passive accumulation approach of the non-targeted, PEG-CPNPs in a solid tumor that is within the abdominal cavity of the mouse. Once the tumors established (one week), CPNPs (diluted into sterile isotonic saline) were administered by tail vein injection (equal ICG concentrations as determined by absorption spectroscopy), and routine images were taken over a 96 hour period. This experiment was repeated at least four times.

Results and Discussion

Physical Characterization of Nanoparticles

The physical characteristics of CPNPs are summarized in Figures 4 and 5. Citrate functionalized CPNPs were utilized as a platform for avidination, which allowed the characterization of avidination via zeta potential analysis (Figure 4A). Figure 4A shows the zeta potential distribution of citrate-CPNPs prior to bioconjugation with avidin (Figure 4A, blue line), and the zeta potential distribution of the avidin-CPNPs complex, which results after the bioconjugation of citrate-CPNPs with avidin (Figure 4A, green line). Prior to bioconjugation with avidin, the citrate-CPNPs displayed a fairly negative mean zeta potential value of -16 $\pm$ 1.3 mV, which is consistent with previous reports (Morgan et al., 2008). However, after bioconjugation with avidin, the avidin-CPNPs displayed a relatively high positive mean zeta potential value of +29 $\pm$ 8.7 mV. The isoelectric point for avidin is pH 10. Thus, the shift from a negative zeta potential to a positive zeta potential distribution is strong evidence of avidin bioconjugation on the surface of CPNPs. However, the zeta potential distribution results, alone, only imply that avidin has been conjugated to the surface of the CPNPs.

Further characterization was used to confirm the presence and bioactivity of avidin. A 2,6-ANS titration was used to confirm both the presence of avidin and its

associated bioactivity. An analysis of the particle size distributions of the nanoparticles via dynamic light scattering (DLS) revealed that all the various bioconjugated CPNPs had a larger mean hydrodynamic diameter than the non-bioconjugated citrate-CPNPs (Figure 4B). Transmission electron microscopy (TEM) analysis indicated that the inorganic particle size was in the range from 10 to 30 nm for all of the CPNPs (Figure 5). The smaller size via TEM relative to DLS analyses is consistent with the ability to determine the solid material diameter via the former technique in contrast to DLS which gives size distribution in colloidal suspension of solid particle, organic layers, and surrounding liquid.

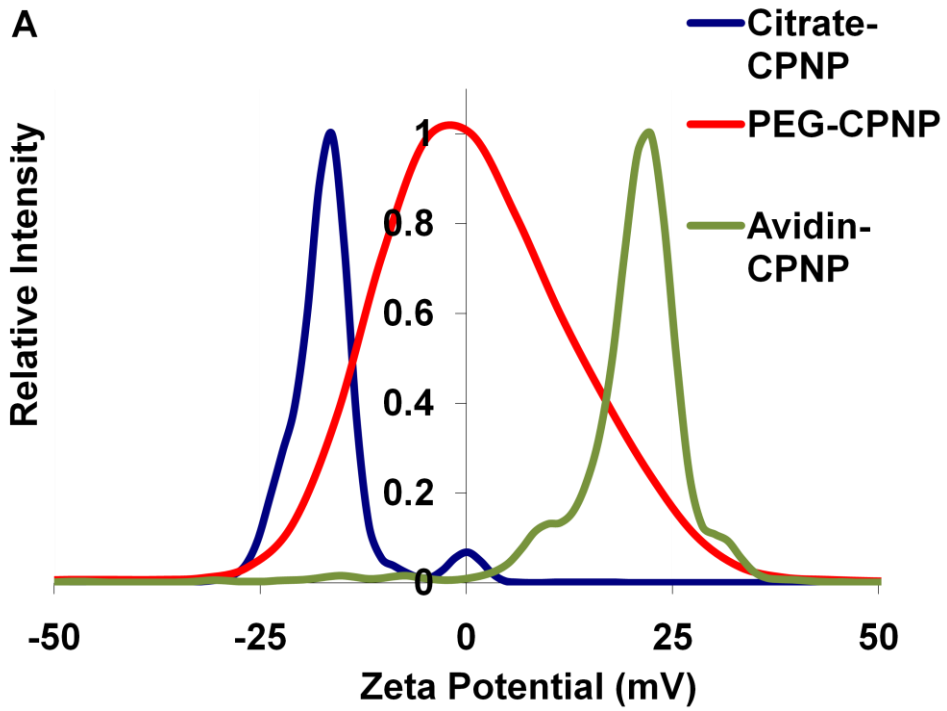

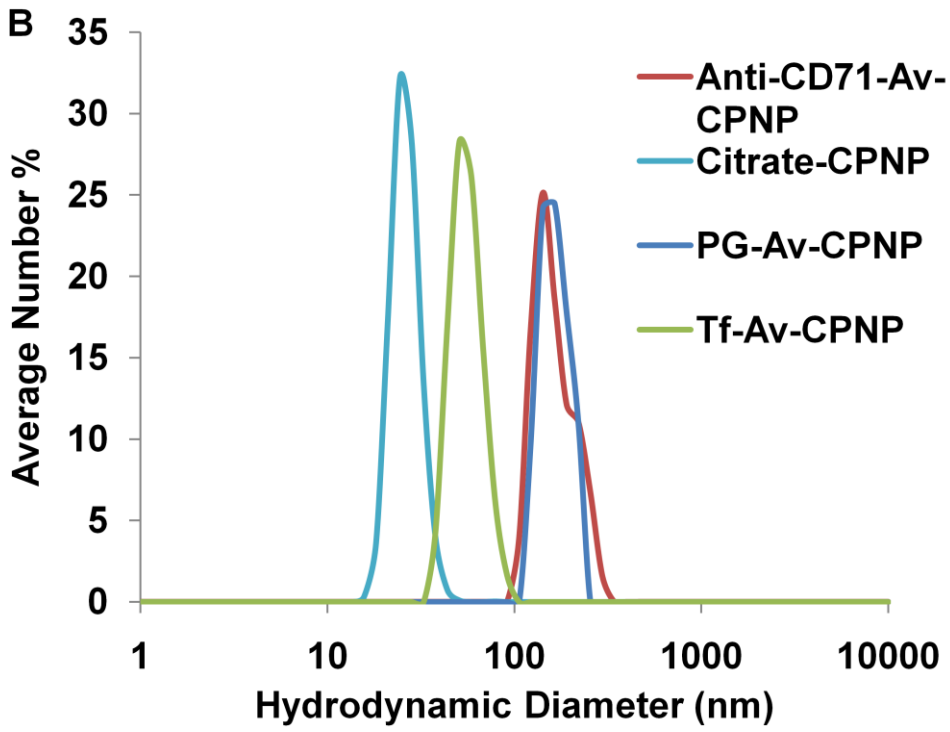

Figure 4. A: Zeta potential distributions for citrate-CPNPs, PEG-CPNPs, and avidin-CPNPs. The citrate-CPNPs (blue line) displayed a mean zeta potential of -16 ± 1.3 mV, whereas, the avidin-CPNPs (green line) had a mean zeta potential value of +29 ± 8.7 mV. In some cases, the zeta potential was as high as +39.8 ± 5.5 mV. The PEG-CPNPs (red line) displayed a mean zeta potential of +3.0 ± 2.0 mV. All zeta potential distributions are representative of three independent experiments. B: Dynamic light scattering determinations for citrate-CPNP, Anti-CD71-Av-CPNP: Anti-CD71-Avidin-CPNPs, PG-Av-CPNP: Pentagastrin-Avidin-CPNPs, and Tf-Av-CPNP: Human Holotransferrin-Avidin-CPNPs. All dynamic light scattering determinations are the mean of three independent experiments.

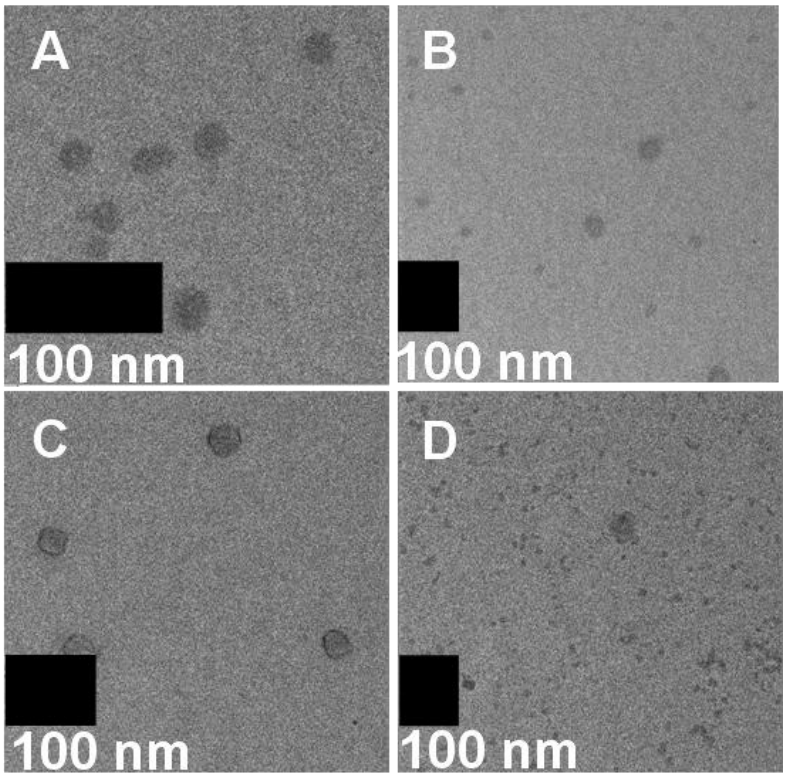

Figure 5. TEM images of A: Citrate-CPNPs; B: Anti-CD71-Avidin-CPNPs; C: Human Holotransferrin-Avidin-CPNPs; D: Pentagastrin-Avidin-CPNPs.

Previous studies have demonstrated that a 2,6-ANS assay can be utilized to accurately quantify avidin (Mock et al., 1985). The 2,6-ANS fluorescent probe will also bind to avidin, an event that can be measured by fluorescence spectroscopy. Figures 6A and 6B show the results for the first step of the two-step 2,6-ANS assay. Without avidin present, the 2,6-ANS fluorescent probe displays minimal fluorescence. However, in the presence of avidin, the binding of 2,6-ANS to the biotin binding site on avidin produces an increase in fluorescence intensity. The 2,6-ANS was therefore added in increasing concentrations to the avidin-CPNPs, and a

concentration-dependent increase in 2,6-ANS fluorescence emission was noted (Figures 6A and 6B). The titration of 2,6-ANS showed an increase in fluorescence up to 1.79×10^{6} RFU after the addition of 3.40×10^{-5} M 2,6-ANS. Beyond this point of maximum fluorescence intensity the 2,6-ANS self-quenched, at which point biotin was added to displace the 2,6-ANS. Figures 6C and 6D show the results for the titration of biotin to displace the 2,6-ANS. Biotin has a greater affinity for the biotin binding site on avidin than does the 2,6-ANS fluorescent probe. Therefore, the addition of biotin to the 2,6-ANS-Avidin-CPNP complex results in the displacement of 2,6-ANS by biotin from the biotin binding site on avidin. Since the 2,6-ANS fluorescent probe displays minimal fluorescence when it is not bound to avidin, this displacement produces a decrease in fluorescence (Figures 6C and 6D) to a plateau of 1.08×10^{6} RFU after the addition of 1.90×10^{-9} mol biotin. The plateau is present because of the intrinsic fluorescence of 2,6-ANS. This result demonstrates the successful coupling of biotin to the avidin-CPNPs. The 2,6-ANS fluorescence emission did not decrease completely as some 2,6-ANS remains bound to avidin-CPNPs. The affinity of avidin for biotin is high. However, concentrations of reactants and ionic conditions can influence this affinity as it has been established that water participates in displacing biotin from the binding pocket of avidin, or similar proteins. Nonetheless, this analysis has successfully demonstrated that the avidin-CPNPs are biofunctional, through binding of 2,6-ANS as well as its displacement by biotin.

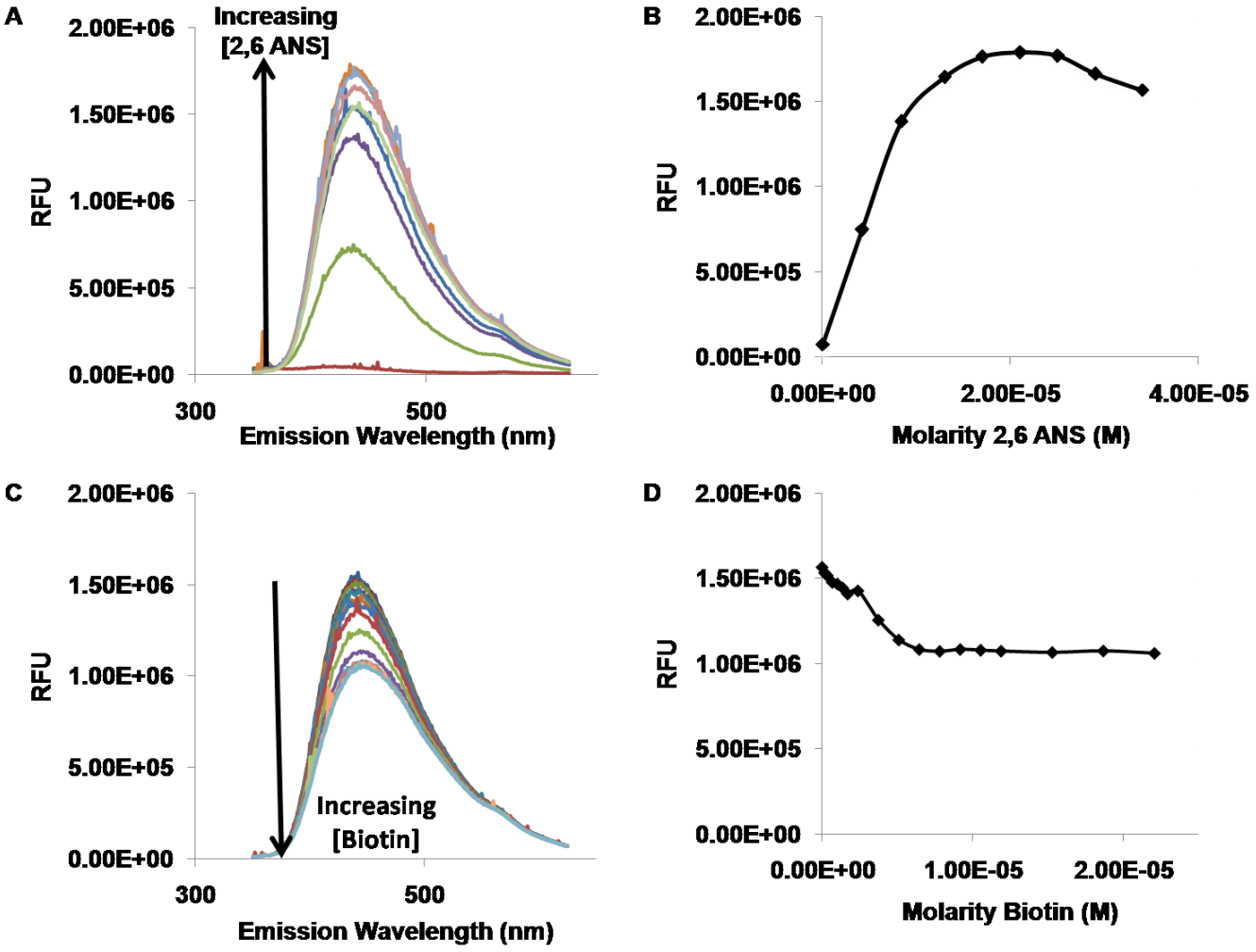
A
Increasing
[2,6 ANS]
2.00E+06
1.50E+06
1.00E+06
5.00E+05
0.00E+00
RFU
300
500
Emission Wavelength (nm)
B
2.00E+06
1.50E+06
1.00E+06
5.00E+05
0.00E+00
RFU
0.00E+00
2.00E-05
4.00E-05
Molarity 2,6 ANS (M)
C
2.00E+06
1.50E+06
1.00E+06
5.00E+05
0.00E+00
RFU
Increasing
[Biotin]
300
500
Emission Wavelength (nm)
D
2.00E+06
1.50E+06
1.00E+06
5.00E+05
0.00E+00
RFU
0.00E+00
1.00E-05
2.00E-05
Molarity Biotin (M)

Figure 6. The displacement of 2,6-ANS was utilized to evaluate the coupling of biotin to avidin-CPNPs. A: Fluorescence intensities for the first step of the 2,6-ANS assay. The addition of 2,6-ANS to the avidin-CPNP complex results in a six fold increase in fluorescence as the fluorescent probe binds to the biotin binding site on avidin. The 2,6-ANS was added at increasing concentrations to avidin-CPNPs and increased fluorescence, indicative of 2,6-ANS bound to avidin, was quantitatively determined. B: Peak height of fluorescence shown on Figure 6A as a function of 2,6-ANS molarity. C: Fluorescence intensities for the second step of the 2,6-ANS assay. The addition of biotin to the 2,6-ANS-Avidin-CPNP complex results in a decrease in fluorescence as biotin displaces the fluorescent probe from the biotin binding site on avidin. Biotin was added at increasing concentrations to the 2,6-ANS-Avidin-CPNP complex and a decrease in fluorescence, indicative of biotin displacing 2,6-ANS, was quantitatively determined. D: Peak height of fluorescence shown on Figure 6C as a function of biotin molarity. All determinations are representative of three independent experiments.

The calculations based on the 2,6-ANS assay indicate that 1×10^{15} biotin binding sites are present. Theoretically, each avidin tetramer has 4 biotin binding sites in solution. However, only 2 to 3 biotin binding sites have been found to be biofunctional and capable of binding to biotin in a given time (Mock et al., 1985). In addition, the conjugation of avidin to CPNPs reduces the avidin surface area and potentially the number of biotin binding sites available for biotin binding. Therefore,

assuming that each avidin molecule has 2 biofunctional biotin binding sites, about 5.7×10^{14} avidin molecules are present. There are approximately 6×10^{14} CPNPs/ml based on fluorescence correlation spectroscopy (Morgan et al., 2008; Muddana et al., 2009). This indicates on average there is ~1 avidin conjugated per CPNP.

In Vivo Evaluation of Nanoparticles

Regarding the evaluation of breast cancer-targeted CPNPs *in vivo* (Figure 7), it has been previously shown that the non-targeted, PEG-CPNPs passively accumulated in breast cancer tumors via an enhanced permeation and retention effect (Altinoğlu et al., 2008). This finding was successfully repeated within this trial as a positive control. Intriguingly, only tumors from mice receiving Anti-CD71-Avidin-CPNPs, and not Human Holotransferrin-Avidin-CPNPs, were effectively targeted. It has been reported, and is likely in this circumstance, that the transferrin receptors are saturated with transferrin and therefore are unable to bind the Human Holotransferrin-Avidin-CPNPs. This is also supported by the success of the Anti-CD71-Avidin-CPNPs, which recognize an epitope separate from the ligand-binding site on the transferrin receptor. Importantly, the Anti-CD71-Avidin-CPNPs were more effective at targeting the tumors than the passively accumulating PEG-CPNPs based on the relative fluorescence intensity. However, and not surprisingly, the effective targeting was not limited to the tumors, but also to the spleen which is rich in a diversity of hematopoietic cells. It was observed that the nanoparticles were generally slower to clear the animal, indicated by some staining of fecal material moving through the intestine (data not shown), a clearance mechanism that has been previously reported (Altinoğlu et al., 2008). It was also observed that there was some off-target staining of the stomach (confirmed following necropsy), likely due

to avidin interaction with biotin ingested as part of the mouse's diet. Overall, these findings showed that the transferrin receptor-targeted CPNPs were effective and selective in an *in vivo* model of breast cancer.

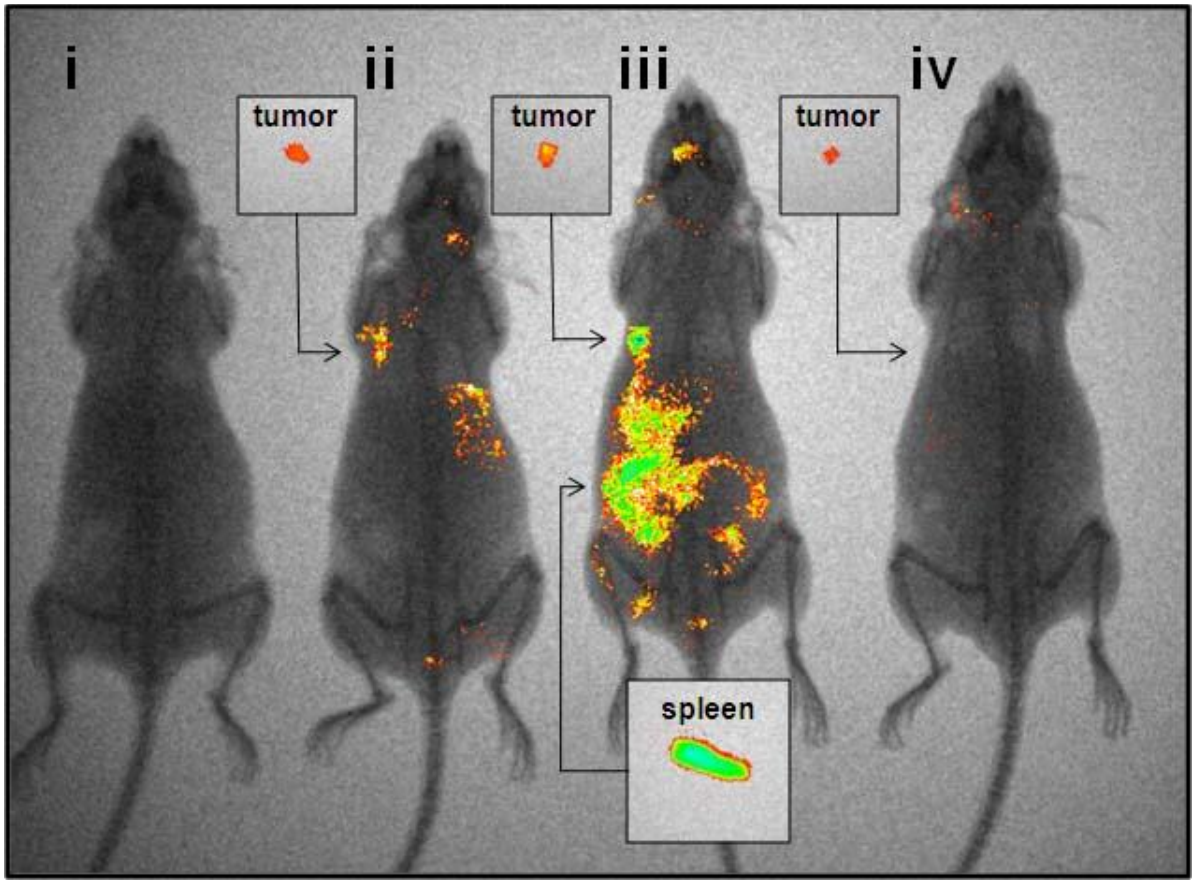

Figure 7. Targeting transferrin receptors in an *in vivo* subcutaneous-tumor model of breast cancer. Human MDA-MB-231 metastatic breast cancer cells were xenografted subcutaneously into athymic nude mice. One week following engraftment, ICG-loaded CPNPs were administered systemically via tail vein injection and near-infrared images were taken 96 hours post-injection. From left to right, mice receiving: (i) free ICG, (ii) ICG-loaded, PEG-CPNPs, (iii) ICG-loaded,

Anti-CD71-Avidin-CPNPs, or (iv) ICG-loaded, Human Holotransferrin-Avidin-CPNPs. Inserts: excised tumors (mice ii, iii, and iv), excised spleen (mouse iii). All images are representative of four independent experiments.

From the evaluation of pancreatic cancer-targeted CPNPs *in vivo* (Figure 8), it was found that the non-targeted, PEG-CPNPs effectively accumulated within the small BxPC-3 tumors within the pancreas, and these whole animal images were confirmed by excision of the pancreas. The Pentagastrin-Avidin-CPNPs, using the avidin-biotin coupling approach, also targeted the pancreatic tumors, as well as the gastrin receptor-rich stomach. However, the Gastrin-10-PEG-CPNPs proved to be much more successful at targeting the pancreatic tumors, the stomach, and even the brain which is also rich in gastrin receptors. An advantage of the later targeting approach is the covalent attachment, eliminating the possibility of non-specific avidin interactions *in vivo*, as well as the PEG which allows for improved systemic retention and decreased immune-reactivity. It is also likely, that the presence of avidin on the CPNPs is not permissive to crossing the blood-brain-barrier, whereas the PEG-maleimide coupling is. It is noteworthy that the untargeted, PEG-CPNPs did not display any significant brain-accumulation in this study. A recent study comparing interleukin-13-targeted nanoliposomes to untargeted nanoliposomes in a cranial model of glioblastoma showed that only targeted nanoliposomes moved significantly across the blood-brain-barrier **(**Madhankumar et al., 2009). The current study, although using a different target and different nanoparticles (gastrin receptor-

targeted CPNPs), corroborates the other group's finding that targeted nanoparticles can cross the blood-brain-barrier. Importantly, the CPNPs are biocompatible and it has been previously shown that they exhibited no specific detrimental effects toward neurons (Kester et al., 2008). This was reiterated in the current study, as no mice receiving any CPNPs showed signs of neurological deficits. Therefore, this portion of the study demonstrated that the CPNPs can be effectively targeted to gastrin receptors *in vivo* in a model of pancreatic cancer, and further showed the potential for targeting across the blood-brain-barrier.

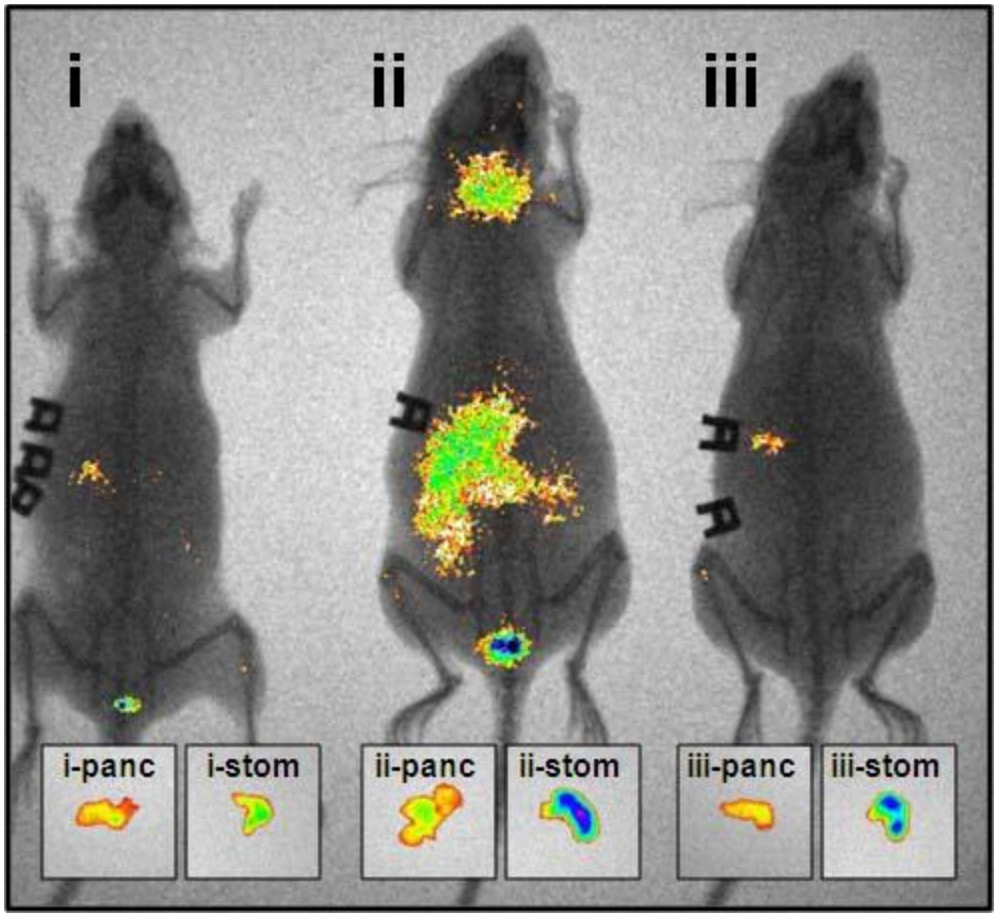

Figure 8. Targeting gastrin receptors in an *in vivo* orthotopic-tumor model of pancreatic cancer. Human BxPC-3 pancreatic cancer cells were xenografted orthotopically into athymic nude mice. One week following engraftment, ICG-loaded CPNPs were administered systemically via tail vein injection and near-infrared images were taken 96 hours post-injection. From left to right, mice receiving: (i) ICG-loaded, PEG-CPNPs, (ii) ICG-loaded, Gastrin-10-PEG-CPNPs (covalently coupled), or (iii) ICG-loaded, Pentagastrin-Avidin-CPNPs. Respective inserts to all mice: (panc) excised, tumor-bearing, pancreas, and (stom) excised stomach. All images are representative of at least four independent experiments.

Conclusions

The ability to target nanodelivery systems to specific tissues is important to the development of better therapeutics for diseases such as cancer. In many studies and clinical circumstances, the efficacies of treatments are limited or the off-target effects are dramatic. Nanoscale therapeutics help to minimize these problems by concentrating smaller doses of therapeutic agents yet are still limited if not targeted. Recent research has shown that molecularly-specific therapeutics, or targeted therapeutic delivery systems are highly efficacious, and may even help to overcome complicating circumstances such as multidrug resistance. The CPNPs in this study were engineered specifically as non-toxic biocompatible nanoscale delivery vehicles. It has been previously shown that a variety of molecules, including dyes that could be used in tumor detection, or hydrophobic antineoplastic agents such as ceramide could be encapsulated (Morgan et al., 2008; Altinoğlu et al., 2008; Kester et al., 2008). Until now, the CPNPs have relied on passive accumulation via enhanced permeation retention effect, to 'target' solid tumors. This study demonstrates that surface targeting strategies can be successfully attached to the CPNPs, via two distinct coupling methods, and these bioconjugated CPNPs can effectively target select tissues. Specifically, breast cancer tumors were targeted *in vivo* by targeting transferrin receptors, and orthotopic pancreatic cancer tumors were targeted *in vivo* by targeting gastrin receptors. This study also showed that gastrin receptor-targeted

CPNPs could cross the blood-brain-barrier, which may expand the utility of the CPNPs to therapeutics targeted to glioblastoma or even to neurodegenerative or psychiatric disorders. This study also confirmed that the non-targeted, PEG-CPNPs could accumulate, and could be effectively imaged, within small orthotopic pancreatic tumors, extending the diagnostic imaging capability and therapeutic delivery capabilities to one of the more evasive cancers. Altogether, this study showed the successful conjugation of surface targeting strategies to the CPNPs, demonstrating the effectiveness, selectivity, and utility in two separate *in vivo* models. This study will allow the further development of the CPNPs to target a diversity of disorders, including several poor prognosis cancers and possibly even non-solid tumors such as leukemia.

References

Altinoğlu EI, Russin TJ, Kaiser JM, Barth BM, Eklund PC, Kester M, Adair JH. Near-infrared emitting fluorophore-doped calcium phosphate nanoparticles for *in vivo* imaging of human breast cancer. ACS Nano. 2008 Oct 28;2(10):2075-84.

Bajpai PK, Benghuzzi HA. Ceramic systems for long term delivery of chemicals and biologicals. J Biomed Mater Res. 1988;22:1245-66.

Barroug A, Fastrez J, Lemaitre J, Rouxhet PG. Adsorption of succinylated lysozyme on hydroxyapatite. J Colloid Interface Sci. 1997;189:37-42.

Barroug A, Glimcher M. Hydroxyapatite crystals as a local delivery system for cisplatin: adsorption and release of cisplatin *in vitro*. J Orthop Res. 2002;20:274-80.

Barroug A, Lemaitre J, Rouxhet PG. Influence of crystallite size on the surface properties of calcium-deficient hydroxyapatites. J Alloys Comp. 1992;185:152-6.

Barroug A, Lemaitre J, Rouxhet PG. Lysozyme on apatites: a model of protein adsorption controlled by electrostatic interactions. Colloids Surf. 1989;37:339-55.

Daniels TR, Delgado T, Helguera G, Penichet ML. The transferrin receptor part II:

targeted delivery of therapeutic agents into cancer cells. Clin Immunol. 2006a;121(2):159-76.

Daniels TR, Delgado T, Rodriguez JA, Helguera G, Penichet ML. The transferrin receptor part I: biology and targeting with cytotoxic antibodies for the treatment of cancer. Clin Immunol. 2006b;121(2):144-58.

De Groot K, Klein CPAT, Wolke JGC, de Blieck-Hogervors JMA. Chemistry of calcium phosphate bioceramics. CRC Press: Boca Raton, 1990;3–17.

Kester M, Heakal Y, Fox T, Sharma A, Robertson GP, Morgan TT, Altinoğlu EI, Tabaković A, Parette MR, Rouse SM, Ruiz-Velasco V, Adair JH. Calcium phosphate nanocomposite particles for in vitro imaging and encapsulated chemotherapeutic drug delivery to cancer cells. Nano Lett. 2008 Dec;8(12):4116-21.

Madhankumar AB, Slagle-Webb B, Wang X, Yang QX, Antonetti DA, Miller PA, Sheehan JM, Connor JR. Efficacy of interleukin-13 receptor-targeted liposomal doxorubicin in the intracranial brain tumor model. Mol Cancer Ther. 2009 Mar;8(3):648-54.

Magne D, Faucheux C, Grimandi G, Daculsi G, Guicheux J. Calcium phosphate ceramics as carriers for bone therapeutic agents. Drug Disc Today 2002;7(17):928-31.

Mock DM, Langford G, Dubois D, Criscimagna N, Horowitz P. A fluorometric assay for the biotin-avidin interaction based on displacement of the

fluorescent probe 2-anilinonaphthalene-6-sulfonic acid. Anal Biochem. 1985 Nov 15;151(1):178-81.

Morgan TT, Muddana HS, Altinoğlu EI, Rouse SM, Tabaković A, Tabouillot T, Russin TJ, Shanmugavelandy SS, Butler PJ, Eklund PC, Yun JK, Kester M, Adair JH. Encapsulation of organic molecules in calcium phosphate nanocomposite particles for intracellular imaging and drug delivery. Nano Lett. 2008 Dec;8(12):4108-15.

Muddana HS, Morgan TT, Adair JH, Butler PJ. Photophysics of Cy3-encapsulated calcium phosphate nanoparticles. Nano Lett. 2009 Apr;9(4):1559-66.

Omary MB, Trowbridge IS, Minowada J. Human cell-surface glycoprotein with unusual properties. Nature 1980;286:888–91.

Panyam J, Labhasetwar V. Biodegradable nanoparticles for drug and gene delivery to cells and tissue. Adv Drug Deliv Rev. 2003;55(3):329-47.

Rouse SM. Synthesis and properties of unagglomerated nanocomposite particles for nanomedical applications. (PhD dissertation, Pennsylvania State University, 2006).

Shindelman JE, Ortmeyer AE, Sussman HH. Demonstration of the transferrin receptor in human breast cancer tissue. Potential marker for identifying dividing cells. Int. J. Cancer 1981;27:329–34.

Smith JP, Fantaskey AP, Liu G, Zagon IS. Identification of gastrin as a growth peptide in human pancreatic cancer. Am J Physiol. 1995 Jan;268(1 Pt 2):R135-41.

Smith JP, Stock EA, Wotring MG, McLaughlin PJ, Zagon IS. Characterization of the CCK-B/gastrin-like receptor in human colon cancer. Am J Physiol. 1996 Sep;271(3 Pt 2):R797-805.

Sutherland R, Delia D, Schneider C, Newman R, Kemshead J, Greaves M. Ubiquitous cell-surface glycoprotein on tumor cells is proliferation-associated receptor for transferrin. Proc. Natl. Acad. Sci. U.S.A. 1981;78:4515–19.

Tung MS. Calcium phosphates: structure, composition, solubility, and stability. In calcium phosphates in biological and industrial systems, Amjad Z., Ed. Kluwer Academic Publishers: Boston, 1998;1-19.

Wank SA, Pisegna JR, de Weerth A. Brain and gastrointestinal cholecystokinin receptor family: structure and functional expression. Proc Natl Acad Sci U S A. 1992 Sep 15;89(18):8691-5.